Available online at www.sciencedirect.com
ScienceDirect
Acta Materialia 57 (2009) 5621–5631
Acta MATERIALIA
www.elsevier.com/locate/actamat

Modeling equiaxed solidification with melt convection and grain sedimentation—I: Model description

M. Wu *, A. Ludwig

Simulation and Modeling of Metallurgical Processes, Department of Metallurgy, University of Leoben, A-8700 Leoben, Austria

Received 2 October 2008; received in revised form 10 July 2009; accepted 28 July 2009
Available online 27 August 2009

Abstract

Part I of this two part investigation presents a modified volume-averaged equiaxed solidification model which accounts for nucleation, globular grain growth, globular-to-dendritic transition, dendritic growth, formation of extra- and interdendritic eutectic, grain transport and melt convection, and their influence on microstructure and macrosegregation. Globular grain growth is governed by diffusion around a spherical grain. For the dendritic growth, a "natural" grain envelope smoothly enclosing the primary and secondary dendrite tips is assumed to separate the interdendritic melt from the extradendritic melt. The solid dendrites and interdendritic melt, confined in the "natural" grain envelope, combine to form a dendritic grain. Two "hydrodynamic" phases are considered: the extradendritic melt and the equiaxed grains; and three thermodynamic phase regions are distinguished: the solid dendrites, the interdendritic melt and the extradendritic melt. The velocities of the hydrodynamic phases are solved with a two-phase Eulerian approach, and transport of the mass and solute species of each thermodynamic phase region are considered individually. Growth kinetics for the grain envelope and the interdendritic melt solidification are implemented separately. Simplification of the grain dendritic morphology and treatment of the non-uniform solute distribution in the interdendritic melt region are detailed. Illustrative modeling results and model verification are presented in Part II.
© 2009 Acta Materialia Inc. Published by Elsevier Ltd. All rights reserved.

Keywords: Modeling; Solidification; Dendrite; Convection; Sedimentation

1. Introduction

Modeling equiaxed solidification at the process scale is still a challenging topic, owing to the complexity of global multiphase transport phenomena coupled with microscopic solidification kinetics. One of the most promising models for equiaxed dendritic solidification, the micro-macro model or solute diffusion model, was proposed by Rappaz and Thévoz (RT) [1,2] and further improved upon by many authors [3–12]. The basic idea behind the RT model is to solve the global energy conservation equation by considering the solidification kinetics that occur at the microscopic scale.

In the RT model, the nucleation of the grain and its dendritic growth are assumed to occur in an "isolated spherical cell", which is also regarded as an isolated representative volume. No mass or species exchange is considered between the neighboring representative volumes. The spherical cell/volume is subdivided into three distinct thermodynamic phase regions: the solid dendrite (s), the interdendritic melt (d) enclosed within the envelope of the grain, and the extradendritic melt (ℓ) outside the envelope. The envelope of the grain is set as a fictitious spherical surface "stretched" by the primary dendritic tips. The evolution of the grain envelope is determined by the tip growth kinetics. A uniform interdendritic melt is assumed, and its concentration is identical to the thermodynamic equilibrium concentration determined by the local temperature and the thermodynamic phase diagram. The solidification of the interdendritic melt within the grain envelope is deduced

* Corresponding author. Tel.: +43 3842 4023103; fax: +43 3842 4023102.
E-mail address: menghuai.wu@mu-leoben.at (M. Wu).

1359-6454/$36.00 © 2009 Acta Materialia Inc. Published by Elsevier Ltd. All rights reserved.
doi:10.1016/j.actamat.2009.07.056

Nomenclature

c_0 initial (nominal) composition of alloy (wt.%)
c_E eutectic concentration (wt.%)
c_e average concentration in equiaxed grains (wt.%)
$\bar{c}_{env}$ average concentration at grain envelope (wt.%)
c_ℓ, c_d, c_s species concentrations (wt.%)
c_ℓ^*, c_s^* equilibrium concentration at s–d interface (wt.%)
c_ℓ^{ref} reference concentration (wt.%)
$C_{\ell e}^D$ diffusive species exchange between extradendritic liquid and equiaxed grains (kg m^{-3} s^{-1})
$C_{\ell e}^M$ species exchange at ℓ–e interface due to envelope growth (kg m^{-3} s^{-1})
$C_{\ell d}^M, C_{\ell s}^M$ species transfer from ℓ-phase to d- and s-phases by phase change (kg m^{-3} s^{-1})
$C_{\ell d}^D, C_{\ell s}^D$ species transfer from ℓ-phase to d- and s-phases by diffusion (kg m^{-3} s^{-1})
C_{ds}^M species transfer from d-phase to s-phase by phase change (kg m^{-3} s^{-1})
C_{ds}^D species transfer from d-phase to s-phase by diffusion (kg m^{-3} s^{-1})
c_{mix} mix concentration (l)
$c_p^\ell, c_p^d, c_p^s, c_p^e$ specific heat (J kg^{-1} K^{-1})
D_ℓ, D_s diffusion coefficient (m^2 s^{-1})
d_e average diameter of e-phase (equiaxed grain diameter) (m)
d_2 diameter of second dendrite arm (m)
$\vec{F}_{Be}$ buoyancy force of equiaxed phase (kg m^{-2} s^{-2})
$F_{B\ell}$ thermal buoyancy force of extradendritic melt (kg m^{-2} s^{-2})
f_ℓ, f_s, f_d volume fraction of ℓ-, s- and d-phases (l)
$f_e = f_s + f_d$ volume fraction of e-phase (l)
f_s^e, f_d^e volume fraction of s- and d-phase regions within e-phase (l)
f_e^c equiaxed grain packing limit (l)
$f_{Eu}^{total}, f_{Eu}^{extra}, f_{Eu}^{intern}$ volume fraction of total, extra- and interdendritic eutectic phases (l)
$\vec{g}$ gravity (m s^{-2})
H^* volume heat transfer coeff. between extradendritic melt and grain envelope (W m^{-3} K^{-1})
h_ℓ, h_e enthalpy (J kg^{-1})
h_ℓ^{ref}, h_e^{ref} reference enthalpy (J kg^{-1})
J_ℓ species diffusive flux in extradendritic melt (m s^{-1})
J_s species diffusive flux in interdendritic solid (m s^{-1})
$K_{\ell e} (= K_{e\ell})$ liquid-equiaxed drag coefficient (kg m^{-3} s^{-1})
k solute partitioning coefficient at the s–d interface (l)
k_e, k_s, k_d, k_ℓ thermal conductivity (W m^{-1} K^{-1})
L latent heat of solidification (J kg^{-1})
l_d diffusion length in interdendritic melt (m)
l_ℓ diffusion length in extradendritic melt (m)
l_s diffusion length in interdendritic solid (m)
$M_{\ell e} (= -M_{e\ell})$ liquid-equiaxed net mass transfer rate (kg m^{-3} s^{-1})
M_{ds} interdendritic solidification rate (kg m^{-3} s^{-1})
$M_{\ell s}, M_{\ell d}$ mass transfer rate from extradendritic melt to s- and d-phases (kg m^{-3} s^{-1})
M slope of liquidus in phase diagram (K)
N_e equiaxed grain production rate by nucleation (m^{-3} s^{-1})
n equiaxed grain number density (m^{-3})
n_{max} maximum equiaxed grain density, or maximum available nucleation sites in simultaneous nucleation law (m^{-3})
p pressure (N m^{-2})
$Q_{\ell e}^D (= -Q_{e\ell}^D)$ energy transfer between extradendritic liquid and equiaxed (J m^{-3} s^{-1})
Q_ℓ^M, Q_e^M energy source terms to treat the latent heat (J m^{-3} s^{-1})
R_e radius of grain envelope (m)
R_f maximum radius of a grain envelope (m)
S_e^M surface concentration of the equivalent sphere (m^{-1})
S_e^D diffusion surface concentration of the natual grain contour (m^{-1})
S_s s–d interface concentration (m^{-1})
T, T_ℓ, T_e temperature (K)
T_E eutectic temperature (K)
T_ℓ^{ref} reference temperature for thermal buoyancy force (K)
T_{ref} reference temperature for enthalpy definition (K)
ΔT constitutional undercooling (K)
ΔT_N undercooling for maximum grain production rate (K)
ΔT_σ Gaussian distribution width of nucleation law (K)
t time (s)
Δt time step (s)
$\vec{U}_{\ell e}^D (= -\vec{U}_{e\ell}^D)$ liquid-equiaxed momentum change due to drag force (kg m^{-2} s^{-2})
$\vec{U}_{\ell e}^M (= -\vec{U}_{e\ell}^M)$ liquid-equiaxed momentum exchange due to grain envelope growth (kg m^{-2} s^{-2})
$\vec{u}_\ell, \vec{u}_e$ velocity vector (m s^{-1})
$\Delta \vec{u}$ relative velocity between melt and grains (m s^{-1})
v_{glob} growth velocity of globular grain (m s^{-1})
v_{env} growth velocity of volume-equivalent spherical envelope (m s^{-1})
v_{tip} growth velocity of dendrite tips (m s^{-1})
v_{sd} s–d interface growth velocity (m s^{-1})
v_{R_e} growth velocity of grain envelope (m s^{-1})
β_2 a constant ($\sim$1) in Eq. (33) (l)
β_T thermal expansion coefficient (K^{-1})
β_c solutal expansion coefficient (l)
β_s solidification volume shrinkage (l)
Φ_{Avr}^e Avrami factor for grain impingement (l)

Φ^{s}_{Avr}	Avrami factor for interdendritic solid impingement (l)
Φ_{env}	shape factor of dendritic grain (l)
Φ_{sph}	sphericity of dendritic grain envelope (l)
Γ	Gibbs–Thomson coefficient (m K)
λ_2	secondary dendrite arm space (m)
μ_ℓ, μ_e	viscosity of liquid and (effective) equiaxed phase (kg m^{-1} s^{-1})
μ_{mix}	viscosity of equiaxed-liquid mixture (kg m^{-1} s^{-1})
$\rho_\ell, \rho_d, \rho_s$	density of thermodynamic phases (kg m^{-3})
ρ_e	average density of equiaxed phase (kg m^{-3})
$\rho^{ref}_\ell, \rho^{ref}_e$	reference densities of extradendritic melt and equiaxed phase (kg m^{-3})
$\bar{\bar{\tau}}_\ell, \bar{\bar{\tau}}_e$	stress–strain tensors (kg m^{-1} s^{-1})
Ω	supersaturation (l)

Subscripts

d	interdendritic melt
e	equiaxed grain
ℓ	extradendritic melt
s	interdendritic solid

from the species and energy balances. Although the above model casts light on many experimental facts, such as the formation of extradendritic and interdendritic eutectics, the recalescence, etc., it fails to include melt convection and grain sedimentation. Another drawback is the assumption of the uniform interdendritic melt. In multicomponent systems, the concentrations at the dendrite tip positions must be distinguished from the concentrations within the interdendritic region [8]. Even in the binary system, this assumption would cause error in the prediction of quantities such as the depth of recalescence, especially for coarse-grained alloys [1].

A model which accounts for melt convection and grain sedimentation was first proposed by Wang and Beckermann (WB) [9–12]. In the WB model, the nucleation and dendritic growth events are also assumed to occur in an "enclosed spherical representative volume", but it is not considered isolated. The mass and species exchanges between the volumes by convection and diffusion are included. Similar to the RT model, three different phase regions (s, d and ℓ) are distinguished, and a similar idea is employed to handle the growth kinetics for the grain envelope and the solidification of the interdendritic melt. WB also proposed a treatment for the non-uniform concentration in the interdendritic region [9], but this was not implemented in later models [10–12] for equiaxed solidification with convection and grain sedimentation. They also introduced the concept of flow partitioning between the inter- and extradendritic melt to handle the interdendritic flow. With this concept, it is only necessary to account for two velocity fields: the velocity of the s-phase and the velocity of the mixture of inter- and extradendritic melts; and the slow flow of the interdendritic melt in relation to the solid dendrites can also be considered. This slow interdendritic melt flow might be important in regions where there is a high volume fraction of grains when the grains impinge upon one another and the volume fraction of the extradendritic melt approaches zero. A drawback of this flow partitioning approach is that a set of additional supplementary correlations with empirical parameters are required to determine a flow partitioning tensor.

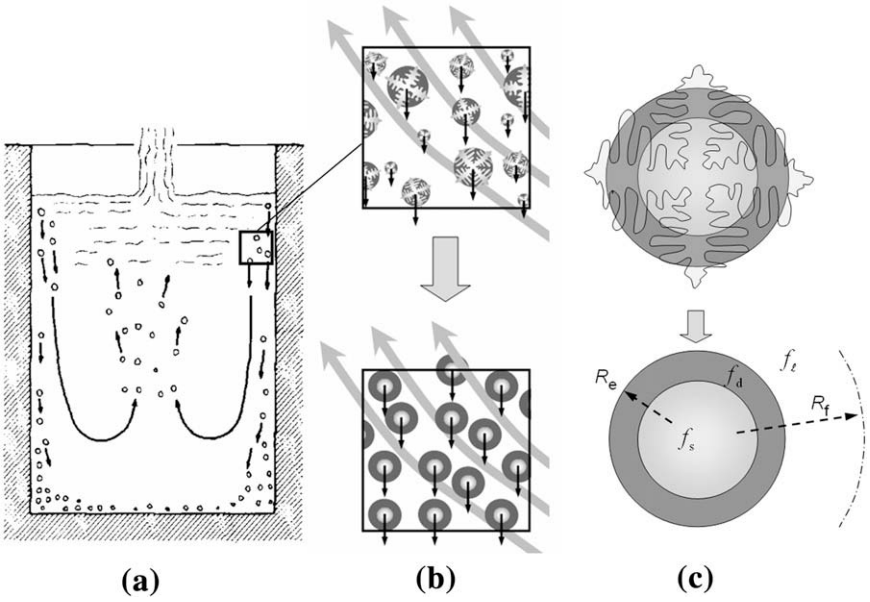

Fig. 1. Schematic of the equiaxed dendritic solidification and dendritic morphology simplifications: (a) melt convection and grain movement at the process scale; (b) construction of the "control volume element" by ignoring the local grain size distribution; (c) use of volume equivalent sphere and solid core to simplify the grain morphological details.

Table 1
Volume-averaged conservation equations of the Eulerian approach for globular/dendritic equiaxed solidification.*

Grain transport: n	$\frac{\partial}{\partial t}n + \nabla\cdot\left(\vec{u}_e n\right) = N_e$ (1)
Mass conservations: f_ℓ, f_e, f_s	$\frac{\partial}{\partial t}(f_\ell\rho_\ell) + \nabla\cdot(f_\ell\rho_\ell\vec{u}_\ell) = M_{e\ell}$ (2)
	$\frac{\partial}{\partial t}(f_e\rho_e) + \nabla\cdot(f_e\rho_e\vec{u}_e) = M_{\ell e}$ (3)
	where $M_{\ell e} = M_{\ell s} + M_{\ell d}$ and $\rho_e = f_s^e\rho_s + f_d^e\rho_d$
	$\frac{\partial}{\partial t}(f_s\rho_s) + \nabla\cdot(f_s\rho_s\vec{u}_e) = M_{ds} + M_{\ell s}$ (4)
Momentum conservations: $\bar{u}_\ell, \bar{u}_e, p$	$\frac{\partial}{\partial t}(f_\ell\rho_\ell\vec{u}_\ell) + \nabla\cdot(f_\ell\rho_\ell\vec{u}_\ell\otimes\vec{u}_\ell) = -f_\ell\nabla p + \nabla\cdot\bar{\bar{\tau}}_\ell + \vec{F}_{B\ell} + \vec{U}_{e\ell}^M + \vec{U}_{e\ell}^D$ (5)
	$\frac{\partial}{\partial t}(f_e\rho_e\vec{u}_e) + \nabla\cdot(f_e\rho_e\vec{u}_e\otimes\vec{u}_e) = -f_e\nabla p + \nabla\cdot\bar{\bar{\tau}}_e + \vec{F}_{Be} + \vec{U}_{\ell e}^M + \vec{U}_{\ell e}^D$ (6)
	where $\bar{\bar{\tau}}_\ell = \mu_\ell f_\ell(\nabla\cdot\vec{u}_\ell + (\nabla\cdot\vec{u}_\ell)^T)$ and $\bar{\bar{\tau}}_e = \mu_e f_e(\nabla\cdot\vec{u}_e + (\nabla\cdot\vec{u}_e)^T)$
Species conservations: c_ℓ, c_e, c_s	$\frac{\partial}{\partial t}(f_\ell\rho_\ell c_\ell) + \nabla\cdot(f_\ell\rho_\ell\vec{u}_\ell c_\ell) = C_{e\ell}^M + C_{e\ell}^D$ (7)
	$\frac{\partial}{\partial t}(f_e\rho_e c_e) + \nabla\cdot(f_e\rho_e\vec{u}_e c_e) = C_{\ell e}^M + C_{\ell e}^D$ (8)
	where $C_{\ell e}^M = C_{\ell d}^M + C_{\ell s}^M$ and $C_{\ell e}^D = C_{\ell d}^D + C_{\ell s}^D$
	$\frac{\partial}{\partial t}(f_s\rho_s c_s) + \nabla\cdot(f_s\rho_s\vec{u}_e c_s) = C_{ds}^M + C_{ds}^D + C_{\ell s}^M + C_{\ell s}^D$ (9)
Enthalpy conservations: h_ℓ, h_e	$\frac{\partial}{\partial t}(f_\ell\rho_\ell h_\ell) + \nabla\cdot(f_\ell\rho_\ell\vec{u}_\ell h_\ell) = \nabla\cdot(k_\ell\nabla\cdot T_\ell) + Q_\ell^M + Q_{e\ell}^D$ (10)
	$\frac{\partial}{\partial t}(f_e\rho_e h_e) + \nabla\cdot(f_e\rho_e\vec{u}_e h_e) = \nabla\cdot(k_e\nabla\cdot T_e) + Q_e^M + Q_{\ell e}^D$ (11)
	where $h_\ell := \int_{T_{ref}}^{T_\ell} c_p^\ell dT + h_\ell^{ref}$ and $h_e := \int_{T_{ref}}^{T_e} c_p^e dT + h_e^{ref}$, $k_e := f_s^e k_s + f_d^e k_d$ and $c_p^e := f_s^e c_p^s + f_d^e c_p^d$

* Note that these 11 partial differential equations are coupled via the transfer terms gathered in Table 2. Together with the fact that f_ℓ and f_e add up to one, Eqs. (1)–(11) are used to compute the 12 quantities: $n, f_\ell, f_e, f_s, \bar{u}_\ell, \bar{u}_e, p, c_\ell, c_e, c_s, h_\ell, h_e$. Here, a conserved vector quantity is considered to be a single variable.

The model proposed in the current paper is a modification and combination of the previous globular and dendritic solidification models. Treatment of flow and grain sedimentation is a continuation of the globular equiaxed model by the authors [13,14]. The current paper is limited to equiaxed solidification, but the extension to mixed columnar–equiaxed solidification [15–17] would be straightforward.

2. Model description and assumptions

As depicted in Fig. 1, equiaxed solidification involves physical phenomena happening at different length scales. Global transport processes occurring at the process scale can be solved with a Eulerian approach based on discretized control volume elements. Each control volume element may contain a number of equiaxed grains. Quantities used to describe nucleation and growth, which occur at a microscopic scale, can be integrated and volume-averaged to formulate source (or exchange) terms to close corresponding transport equations. Note that this volume-averaged approach assumes that all grains within a certain control volume element have the same average size, morphology, velocity, and physical and chemical properties.

2.1. Phase definition and global transport phenomena

(1) Two "hydrodynamic" phases are considered: extradendritic melt (ℓ) and equiaxed grains (e). Their respective volume fractions, f_ℓ and f_e, sum to one and the velocities, $\vec{u}_e$ and $\vec{u}_e$, are calculated with a two-phase Eulerian approach (Eqs. (5) and (6) in Table 1).

(2) According to the RT model [1,2], for dendritic solidification three different thermodynamic phase regions are dis-

Table 2
Mass and species transfer terms.*

	For globular grains	For dendritic grains
Mass transfer ($\ell \rightarrow$ d):	No d-phase present	$M_{\ell d} = v_{R_e} \cdot S_e^M \cdot \rho_d$ (12)
Species transfer ($\ell \rightarrow$ d) by mass transfer:		$C_{\ell d}^M = \bar{c}_{env} \cdot M_{\ell d}$ (13)
Species transfer ($\ell \rightarrow$ d) by diffusion:		$C_{\ell d}^D = -\rho_\ell \cdot S_e^D \cdot J_\ell$ (14)
		with $J_\ell = D_\ell \cdot (\bar{c}_{env} - c_\ell)/l_\ell$, and $l_\ell = D_\ell / v_{R_e}$
Mass transfer ($\ell \rightarrow$ s):	$M_{\ell s} = v_{R_e} \cdot S_e^M \cdot \rho_s$ (15)	No solid forms from extradendritic melt
Species transfer ($\ell \rightarrow$ s) by mass transfer:	$C_{\ell s}^M = c_s^* \cdot M_{\ell s}$ (16)	
Species transfer ($\ell \rightarrow$ s) by diffusion (solid back diffusion):	$C_{\ell s}^D = \rho_s \cdot S_e^D \cdot J_s$ (17)	
	with $J_s = D_s \cdot (c_s^* - c_s)/l_s$ and $l_s = d_e/2$	
Mass transfer (d $\rightarrow$ s):	No d-phase present	$M_{ds} = v_{sd} \cdot S_s \cdot \rho_s$ (18)
Species transfer (d $\rightarrow$ s) by mass transfer:		
Species transfer (d $\rightarrow$ s) by diffusion (solid back diffusion):		$C_{ds}^M = c_s^* \cdot M_{ds}$ (19)
		$C_{ds}^D (= -C_{sd}^D) = \rho_s \cdot S_s \cdot J_s$ (20)
		with $J_s = D_s \cdot (c_s^* - c_s)/l_s$ and $l_s = f_s \cdot \lambda_2/2$

* Note that all transfer terms have to be symmetrical e.g., $M_{\ell d} = -M_{d\ell}, C_{\ell d}^M = -C_{d\ell}^M$, etc.

Table 3
Momentum exchange and other closure laws for the conservation equations.

Nucleation	$N_e = \frac{d\Delta T}{dt} \cdot \frac{n_{max}}{\sqrt{2\pi} \cdot \Delta T_\sigma} \cdot e^{-\frac{1}{2}\left(\frac{\Delta T - \Delta T_N}{\Delta T_\sigma}\right)^2}$	(21)
Momentum exchange ($\ell \leftrightarrow$ e) by mass transfer:	$\vec{U}_{\ell e}^M = \vec{u}^* \cdot M_{\ell e}$ $\vec{u}^* = \begin{cases} \vec{u}_\ell & \text{solidification} \\ \vec{u}_e & \text{re-melting} \end{cases}$	$\vec{U}_{e\ell}^M = -\vec{U}_{\ell e}^M$ (22)
Momentum exchange ($\ell \leftrightarrow$ e) by drag force:	$\vec{U}_{\ell e}^D = K_{\ell e} \cdot (\vec{u}_\ell - \vec{u}_e)$	$\vec{U}_{e\ell}^D = -\vec{U}_{\ell e}^D$ (23)
	$K_{\ell e}$: drag coefficient [13]	
Buoyancy force:	$\vec{F}_{B\ell} = f_\ell \cdot \rho_\ell^{ref} \cdot [1 + \beta_T \cdot (T_\ell^{ref} - T_\ell) + \beta_c \cdot (c_\ell^{ref} - c_\ell)] \cdot \vec{g}$ (24)	
	$\vec{F}_{Be} = f_e \cdot \rho_e^{ref} \cdot (1 + \beta_s \cdot f_s^e) \cdot \vec{g}$ (25)	
	where $\beta_s = (\rho_s - \rho_\ell)/\rho_e^{ref}$	
Enthalpy exchange ($\ell \leftrightarrow$ e) by heat transfer:	$Q_{\ell e}^D = H^* \cdot (T_\ell - T_e)$ $H^* = 10^8$ W/m^3/K (Infinite)	$Q_{e\ell}^D = -Q_{\ell e}^D$ (26)
Latent heat:	$Q_\ell^M = -h_\ell \cdot M_{\ell e} + L \cdot M_{ds} \cdot f_\ell$,	
	$Q_e^M = h_e \cdot M_{\ell e} + L \cdot M_{ds} \cdot f_e$ (27)	
	here $h_\ell = h_e$, latent heat is treated explicitly by source terms	

tinguished: solid dendrites, interdendritic melt and extradendritic melt, indexed s, d and ℓ. Their volume fractions sum to one: $f_s + f_d + f_\ell = 1$. At the s–d interface which separates the solid dendrite (s) from the interdendritic melt (d), thermodynamic equilibrium holds, and solute partitioning occurs. The interdendritic melt (d) is separated from the extradendritic melt (ℓ) by a "natural" grain envelope. The construction of the "natural" grain envelope is detailed in Section 2.2. The volume fraction of the s-phase within a grain envelope is given by $f_s^e = f_s/f_e$, and the volume fraction of d-phase within a grain envelope by $f_d{}^e = f_d/f_e$. In the case of globular solidification, $f_d = 0$ and $f_e = f_s$.

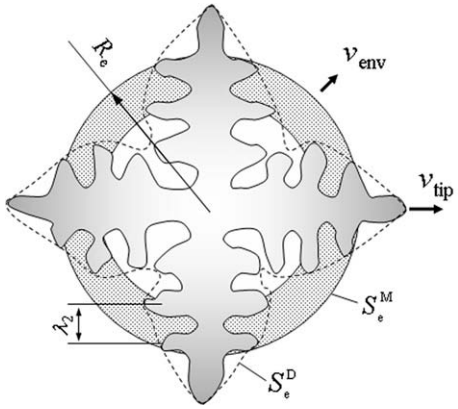

Fig. 2. The shape of the dendritic grain is simplified by an "equivalent sphere". This "equivalent sphere" has the same volume as the "natural" contour around the primary and secondary dendrite tips of the grain (dashed line). The "natural" contour of the grain is also called a "natural" grain envelope.

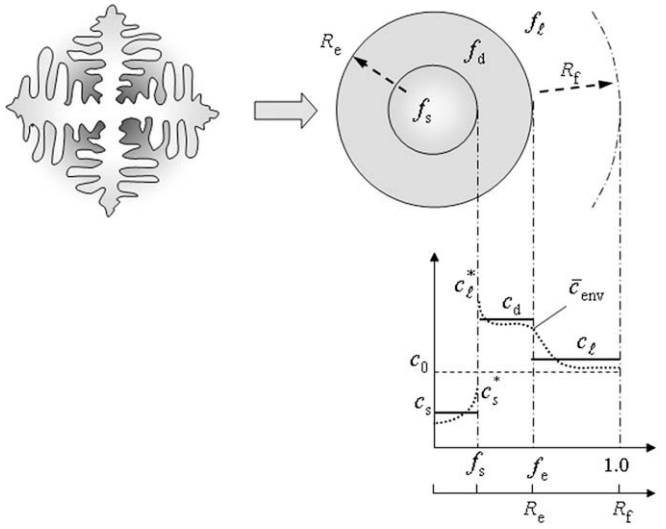

Fig. 3. Model of the species distribution in different phase regions of a growing dendritic grain. The dotted lines represent the species distribution in the different phase regions, and the solid lines represent the averaged concentrations used in the model.

(3) Each control volume contains the extradendritic melt with its average concentration c_ℓ, and may contain several grains (Fig. 1b). For the extradendritic melt, mass and species exchange between the neighboring control volume elements by diffusion and/or melt convection are considered.

(4) The relationships between the thermodynamic and the hydrodynamic phases are as follows. The thermodynamic ℓ-phase is identical to the hydrodynamic ℓ-phase; the thermodynamic s- and d-phases sum up to the hydrodynamic e-phase, i.e., $f_s + f_d = f_e$. Both d- and s-phases share the same velocity field, $\vec{u}_e$.[1]

(5) The transport equations for enthalpy, mass, momentum, species are solved for each hydrodynamic phase (Table 1). In addition, the conservation equation for the grain number density is also solved (Eq. (1) in Table 1). The model using a two-phase Eulerian approach including grain growth, convection and grain movement has been described elsewhere [13,14].

(6) The volume fraction of the equiaxed phase f_e is calculated via mass conservation for the hydrodynamic e-phase according to the grain growth kinetics described in Section 4.1. The solid volume fraction f_s is obtained by solving an additional transport equation which accounts for solidification of the interdendritic melt (Eq. (4) in Table 1).

(7) c_ℓ and c_e are obtained by solving the species conservation equation for each hydrodynamic phase (Eqs. (7) and (8) in Table 1). Here, c_e represents the average solute concentration within the corresponding grains. In addition, the average concentration of the solid is calculated by solving the conservation equation for c_s (Eq. (9) in Table 1). Knowing f_e, f_s, c_e and c_s from solving the corresponding conservation equation, the average concentration of the interdendritic melt c_d can be estimated using the relation $\rho_e f_e c_e = \rho_d f_d c_d + \rho_s f_s c_s$. This differs from previous dendritic solidification models [1–5,10–12], where it was assumed that the averaged interdendritic melt was identical to the thermodynamic equilibrium concentration, $c_d = c_\ell^*$.

(8) The densities of all phases are assumed to be constant and are not equal. The Boussinesq approximation is used to model thermo-solutal convection and grain sedimentation [18].

(9) Two enthalpy equations are solved to calculate T_e and T_ℓ (Eqs. (10) and (11) in Table 1). However, a large (infinite) volume heat exchange coefficient between both hydrodynamic phases is applied to level out any temperature differences ($T_\ell \approx T_e$) [13,15]. Mixture properties, k_e, c_p^e and ρ_e, composed of those of the solid dendrite and the interdendritic liquid are used for the e-phase. Latent heat is explicitly modeled with additional source terms (Eq. (27) in Table 2).

2.2. Microscopic phenomena

(1) A three-parameter heterogeneous nucleation law (Eq. (21) in Table 3) is used to model the nucleation of equiaxed grains [13,19]. This is the source term for the conservation equation of grain number density n (Eq. (1) in Table 1). From the average grain volume f_e/n, an average grain radius is calculated via $4/3\pi R_e^3 = f_e/n$.

(2) An equiaxed grain starts to grow with globular (spherical) morphology, therefore, a Zener-type diffusion field for steady-state growth of a sphere [15,16] is applied in order to calculate the grain growth velocity v_{glob}. As soon as the globular-to-dendritic transition (GDT) occurs, the Lipton–Glicksman–Kurz (LGK) tip growth kinetics [20,21] is applied to estimate the evolution of the grain envelope v_{env}. GDT is assumed to occur when v_{env} exceeds v_{glob} (maximum growth hypothesis).

[1] This assumption might appear too restrictive, especially when considering feeding flow close to the end of solidification. However, in the present approach extradendritic melt can still flow to feed solidification, even above the grain packing limit.

(3) As soon as GDT occurs, the appearance of interdendritic melt is considered, and the dendritic morphology within a grain is simplified by the "equivalent sphere" concept. An "equivalent sphere" consists of a solid core and an interdendritic melt shell (Fig. 2) with a volume equal to the volume enclosed by the natural contour of an actual grain. The growth velocity of the equivalent sphere v_{env} is related to the primary dendrite tip growth velocity v_{tip} by a morphological parameter Φ_{env} (Section 4.1). Knowing the surface concentration of the equivalent spheres $S_{\mathrm{e}}^{\mathrm{M}}$, the mass transfer rate from the ℓ-phase (extradendritic melt) to the e-phase (equiaxed grains) can be calculated. However, it must be noted that the use of $S_{\mathrm{e}}^{\mathrm{M}}$ would underestimate the species transfer by diffusion from the inter- to the extradendritic melt, because the surface area of the natural contour of a grain is larger than the surface area of the equivalent sphere. To handle this discrepancy, a second morphological parameter Φ_{sph} is introduced to determine the "true" surface area of the "natural" contour of the grain $S_{\mathrm{e}}^{\mathrm{D}}$ (see Section 4.1).

(4) The concentration profiles in the different phase regions are shown schematically in Fig. 3. The Eulerian volume-averaged approach accounts only for the averaged concentration of each phase, namely $c_{\mathrm{s}}, c_{\mathrm{d}}, c_{\ell}$. Thermodynamic equilibrium is assumed at the s–d interface, where interface kinetics and curvature effects are neglected. As a result, the equilibrium concentration at the s–d interface, c_{ℓ}^{*}, and that at the dendrite tips are assumed to be comparable. At present, the current model is limited to binary systems. The interface concentration c_{ℓ}^{*} is related to temperature T by the corresponding phase diagram information. The difference between the equilibrium concentration at the s–d interface, c_{ℓ}^{*}, and the averaged interdendritic melt concentration, c_{d}, is the driving force for solidification of the interdendritic melt.

(5) The non-uniform interdendritic solute distribution is modeled following the work of WB [9]. An average concentration at the grain envelope, $\bar{c}_{\mathrm{env}}$, is calculated from the corresponding diffusion flux balance at the grain envelope (see Section 4.3, Eq. (44)). Based on this average envelope concentration, $\bar{c}_{\mathrm{env}}$, the species transfer from the $\ell-$ to the e-phase due to grain growth and diffusive flux is calculated. Note that, if the diffusion length of the extradendritic melt is much larger than the diffusion length of interdendritic melt ($l_{\ell} \gg l_{\mathrm{d}}$), the generally used assumption of $\bar{c}_{\mathrm{env}} = c_{\mathrm{d}}$ would be valid.

(6) Diffusion adjacent to dendrite tips is the governing mechanism for the growth of the primary dendrite tips, i.e., the evolution of the grain envelope, while diffusion adjacent to the s–d interface in the interdendritic melt is the governing mechanism for solidification of the interdendritic melt. The growth of the grain envelope is modeled either according to the Zener-type formulation for the globular growth or according to the LGK tip growth kinetics for the dendritic growth. The diffusion length in the interdendritic region is thought to scale with the secondary arm space λ_2 (see Section 4.2).

(7) For simple binary eutectic alloys, the primary phase solidification ends with the formation of eutectic. For alloys with a small volume fraction of interdendritic eutectic, the formation of eutectic has little influence on the global enthalpy conservation, thus release of eutectic latent heat is neglected. However, as soon as the temperature drops below the eutectic point T_E, the remaining melt solidifies as eutectic, and the primary phase solidification process terminates. As we distinguish between extradendritic and interdendritic melt, we also distinguish between extradendritic eutectic $f_{\mathrm{Eu}}^{\mathrm{extra}}$ and interdendritic eutectic $f_{\mathrm{Eu}}^{\mathrm{intern}}$.

3. Conservation equations

The eleven "transport" quantities, n, $f_{\ell}, f_e, f_s, \vec{u}_{\ell}, \vec{u}_{\mathrm{e}}$, $c_{\ell}, c_e, c_s, h_{\ell}$ and h_{e} (i.e., T_{ℓ}, T_{e}) and pressure p, are obtained by solving the conservation equations together with the condition $f_{\mathrm{e}} + f_{\ell} = 1$, which are summarized in Table 1. Here, a conserved vector quantity is counted only as a single variable. All phases share a single pressure field p. The pressure correction equation is obtained from the sum of the normalized mass continuity equations using the "Phase Coupled SIMPLE (PC-SIMPLE)" algorithm [22]. The mass and species transfer terms used to describe grain growth and solidification are summarized in Table 2. Their derivation is detailed in Section 4. Further closure laws described in previous publications [13–16] are listed in Table 3. The mixture concentration c_{mix}, used as an indicator of macrosegregation, is calculated by the species volume-averaged over all phases [13,14]. To define an artificial "viscosity" of the equiaxed phase μ_{e} (which is needed for the corresponding momentum conservation Eq. (6) in Table 1), the mixing rule $\mu_{\mathrm{mix}} = f_{\ell}\mu_{\ell} + f_{\mathrm{e}}\mu_{\mathrm{e}}$ is applied, where the mixture viscosity μ_{mix} is taken from experimental measurements [23]. As long as f_{e} is small, μ_{e} is in the same order of μ_{ℓ}. As f_{e} approaches the packing limit ($f_{\mathrm{e}}^{\mathrm{c}} = 0.637$), μ_{e} increases to infinity. Beyond $f_{\mathrm{e}}^{\mathrm{c}}$, the e-phase becomes rigid, while the extradendritic melt is still able to penetrate the voids of the closely packed grains.

4. Growth kinetics

4.1. Grain growth

The rate of mass transfer from the ℓ-phase (extradendritic melt) to the e-phase (equiaxed grains) is determined by the growth velocity $v_{R_{\mathrm{e}}}$ and the surface concentration of the volume-equivalent spherical envelope $S_{\mathrm{e}}^{\mathrm{M}}$ (Eq. (12) in Table 3). Two grain morphologies are considered: globular and dendritic. For the globular growth, solute partitioning occurs at the grain envelope which is identical to the solid–liquid interface. The growth velocity of the globular grain v_{glob} is governed by diffusion, and thus a Zener-type growth formulation is used [15]

$$v_{\text{glob}} = \frac{D_\ell}{R_e} \cdot \Omega \tag{28}$$

where $\Omega = (c_\ell^* - c_\ell)/(c_\ell^* - c^*{}_s)$ is the supersaturation.

For dendritic growth (Fig. 2), the growth velocity of the volume equivalent sphere, v_{env}, is related to the dendrite tip velocity v_{tip}. Here, the LGK model [20,21] is implemented for the tip velocity. Thus, one has

$$v_{\text{env}} = \Phi_{\text{env}} \cdot v_{\text{tip}} = \Phi_{\text{env}} \cdot \frac{D_\ell \cdot m \cdot c_\ell^* \cdot (k-1)}{\Gamma \cdot \pi^2} (\text{Iv}^{-1}(\Omega))^2 \tag{29}$$

where the shape factor Φ_{env} correlates the growth velocity of the volume equivalent sphere v_{env} with the primary dendrite tip velocity v_{tip}. If the grain envelope is assumed to be an ideal sphere connecting the outer tips of the primary dendrites [1], Φ_{env} is equal to one. When an octahedral envelope is assumed to connect the primary dendrite tips [5], Φ_{env} is equal to $1/\sqrt[3]{\pi}$. As depicted in Fig. 2, in many cases Φ_{env} can even be smaller than $1/\sqrt[3]{\pi}$. In reality, Φ_{env} is dependent on the type of alloy, the stage of solidification and the relative motion between grains and melt [4,24–27]. Owing to the lack of detailed knowledge on such grain growth, a process-dependent variation of Φ_{env} is not considered here.

In the current model, the morphology transition from globular to dendritic growth (GDT) is determined by comparing the above-mentioned two growth velocities, v_{glob} and v_{env}. At the initial stage, $v_{\text{glob}} > v_{\text{env}}$, and the globular growth model applies. The transition from globular growth to dendritic growth occurs as soon as $v_{\text{env}} \geqslant v_{\text{glob}}$. Therefore, the general formula for the velocity of the volume equivalent sphere can be expressed as

$$v_{R_e} = \max(v_{\text{env}}, v_{\text{glob}}) \tag{30}$$

Using Eq. (30) to handle the GDT is different from the approach described by Appolaire et al. [3,5], where a comparison of two mass transfer rates was proposed (solidification/melting inside the grain was compared with the expansion/shrinkage of the envelope).

The surface concentration S_e^M of the volume equivalent sphere is calculated by

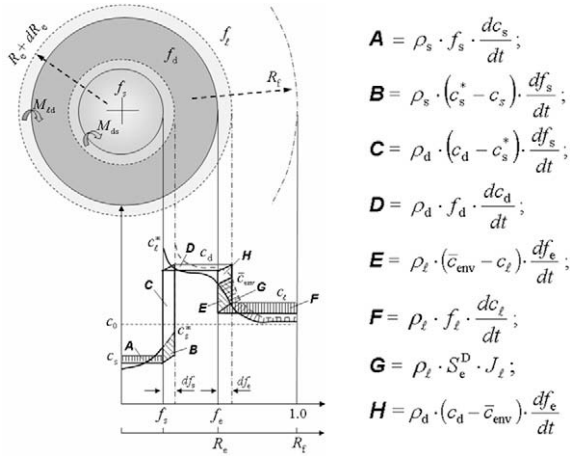

Fig. 4. Concentration redistribution in different phase regions due to growth of the grain envelope and solidification of interdendritic melt.

$$S_e^M = \Phi_{\text{Avr}}^e \cdot (36\pi \cdot n)^{\frac{1}{3}} \cdot f_e^{\frac{2}{3}} \tag{31}$$

where n is the number density of grains, and $\Phi^e{}_{\text{Avr}}$ is an impingement factor which accounts for the effect of impingement of equiaxed grains. In the present paper, it is assumed $\Phi_{\text{Avr}}^e = f_\ell$ (similar to Ref. [15]). Eq. (31) applies for both globular and dendritic solidification. With $v_{R\ e}$ and S_e^M as defined above, the volume-averaged mass transfer rate from the ℓ-to the e-phase can be calculated using Eqs. (12) and (15) in Table 2.

In order to calculate the species exchange between the ℓ- and the e-phase by diffusion, a "diffusion" surface concentration S_e^D is determined by

$$S_e^D = \frac{S_e^M}{\Phi_{\text{sph}}} \tag{32}$$

where $\Phi_{\text{sph}} (\leqslant 1)$ is the sphericity, i.e., the ratio of the surface of the volume equivalent sphere to the surface area of "natural" contour of the grain [28]. In the case of globular grain, or in the case of dendritic grain with its "natural" contour presented with an ideal sphere, Φ_{sph} is equal to one [1]. For a dendritic grain with an octahedral contour, Φ_{sph} is equal to $\sqrt[3]{\pi}/\sqrt{3}$ [5]. For a more general case, as shown in Fig. 2, the "natural" grain envelope is approximated as the contour which connects the primary and secondary dendrite tips. In this case, the value of Φ_{sph} can be much smaller than $\sqrt[3]{\pi}/\sqrt{3}$. In reality, Φ_{sph} may depend on the type of alloy, the stage of solidification and the relative motion between grains and melt as well [4,24–27]. Owing to the lack of information on such details, Φ_{sph} is taken as a constant value. Note that the importance for defining two different morphological parameters, Φ_{env} and Φ_{sph}, are further discussed in Section 4.3.

4.2. Solidification of interdendritic melt

The mass transfer rate from the d- to the s-phase (solidification rate of interdendritic melt) is governed by the s–d interface velocity v_{sd} and the s–d interface concentration S_s. The driving force for v_{sd} is $c_\ell^* - c_d$, but v_{sd} is controlled by diffusion at a diffusion length scale l_d. Following the work of WB [9], take

$$l_d = \beta_2 \cdot \frac{(\lambda_2 - d_2)}{2} \tag{33}$$

where β_2 is a constant on the order of unity (1.0), λ_2 is the secondary dendrite arm spacing, d_2 is the diameter of the secondary dendrite arm, and $\lambda_2 - d_2 = \lambda_2 \cdot f_d^e$, and

$$v_{\text{sd}} = \frac{2 \cdot D_\ell}{\beta_2 \cdot \lambda_2 \cdot f_d^e} \cdot \frac{c_\ell^* - c_d}{c_\ell^* - c_s^*} \tag{34}$$

The s–d interface area in an enclosed grain envelope is also related to the secondary arm spacing ($\propto 2/\lambda_2$). Considering a factor $\Phi_{\text{Avr}}^s (= f_d^e)$ for the impingement of the secondary dendrite arms, the s–d interface concentration can be calculated as:

$$S_s = \frac{2 \cdot \Phi_{\text{Avr}}^s}{\lambda_2} \cdot f_e \tag{35}$$

There is no distinction between the s–d surface and diffusion surface for the interdendritic melt solidification: they are identical. Appolaire et al. suggested another formula for the s–d interface area concentration, but it has yet to be experimentally determined [3–5,29]. The method used to estimate l_d and S_s may seem to be a rough estimation, but the final solidification rate of the interdendritic melt M_{ds}, according to Eqs. (18), (34) and (35), is actually adjusted by $(c_\ell^* - c_d)$, where c_ℓ^* is a function of local temperature. In other words, the final solidification rate is actually indirectly related to the global heat transfer process. The sensitivity of modeling results to l_d and S_s is further studied and discussed in Part II.

4.3. Species exchange between different phase regions

Species exchange between different phase regions was also studied by RT [1] and WB [9]. Without convection, the equiaxed grain can be assumed to solidify in an isolated "representative spherical cell", and the mass and species in the "cell" must be conserved.

The species redistribution due to grain growth and interdendritic melt solidification is shown schematically in Fig. 4. Within a time interval dt, grain growth causes a shell of thickness dR_e to transfer from extradendritic to interdendritic melt, and so the grain volume fraction increases by df_e. The corresponding mass transfer rate is $M_{\ell d}$. While the grain size is increasing, the interdendritic melt may solidify. A new shell of solid with concentration c_s^* forms, in the presently used "equivalent sphere" approach, around the solid core. With that, the solid volume fraction increases by df_s. The corresponding mass transfer rate is M_{ds}.

While the volume equivalent sphere is expanding and the interdendritic melt solidifies, mass and species conservation must be ensured. If one assumes constant but different densities for different phase regions, species conservation is given by

$$\rho_s \frac{d(f_s c_s)}{dt} + \rho_d \frac{d(f_d c_d)}{dt} + \rho_\ell \frac{d(f_\ell c_\ell)}{dt} = 0 \tag{36}$$

The amount of solute in the solid core changes because of the newly formed solid layer ($df_s > 0$) of concentration $c^*{}_s$ when back diffusion is ignored. Thus,

$$\rho_s \frac{d(f_s c_s)}{dt} = \rho_s c_s^* \cdot \frac{df_s}{dt} \tag{37}$$

The amount of solute in the extradendritic region changes as a result of two factors: one is the loss of a layer of the extradendritic melt ($df_\ell < 0$) of concentration $\bar{c}_{env}$ in order to form interdendritic melt, and the other is the gain of solute element by diffusion from the interdendritic melt into the extradendritic melt. Thus,

$$\rho_\ell \frac{d(f_\ell c_\ell)}{dt} = \rho_\ell \bar{c}_{env} \cdot \frac{df_\ell}{dt} + \rho_\ell S_\ell^D J_\ell \tag{38}$$

As the volume fractions of the three phase regions sum up to one ($f_\ell + f_d + f_s = 1$), according to the product rule (Leibniz's law) the second term of the LHS of Eq. (36) can be written

$$\rho_d \frac{d(f_d c_d)}{dt} = -\rho_d c_d \cdot \frac{df_s}{dt} + \rho_d f_d \frac{dc_d}{dt} - \rho_d c_d \cdot \frac{df_\ell}{dt} \tag{39}$$

Inserting Eqs. (37)–(39) into Eq. (36) yields

$$(\rho_s c_s^* - \rho_d c_d) \cdot \frac{df_s}{dt} + \rho_d f_d \frac{dc_d}{dt} + (\rho_\ell \bar{c}_{env} - \rho_d c_d) \cdot \frac{df_\ell}{dt} + \rho_\ell S_\ell^D J_\ell = 0 \tag{40}$$

The meaning of Eq. (40) is obvious. The species rejected at the s–d interface (first term) and the species consumption at the d–ℓ interface (third and fourth terms) lead to the change in the interdendritic concentration (second term).

Note that the back diffusion through the s–d interface into the solid core is ignored in the current approach. Should the back diffusion be considered, Eq. (37) must include a back diffusion term

$$\rho_s \frac{d(f_s c_s)}{dt} = \rho_s c_s^* \cdot \frac{df_s}{dt} + \rho_s S_s J_s \tag{41}$$

and Eq. (40) becomes

$$(\rho_s c_s^* - \rho_d c_d) \cdot \frac{df_s}{dt} + \rho_s S_s J_s + \rho_d f_d \frac{dc_d}{dt} + (\rho_\ell \bar{c}_{env} - \rho_d c_d) \cdot \frac{df_\ell}{dt} + \rho_\ell S_\ell^D J_\ell = 0 \tag{42}$$

This relationship was suggested by many authors [3–7,9] to determine the solidification rate of the interdendritic melt, but with the assumption of complete mixing in the interdendritic melt region, i.e., $c_d = c_\ell^* = \bar{c}_{env}$ and for equal densities (fourth term in Eq. (42) was neglected). However, the current model treats the average interdendritic melt concentration c_d as an additional transport quantity, independent of c_ℓ^*. Depending on the competition between the growth of the grain and the interdendritic solidification, c_d lies between $\bar{c}_{env}$ and c_ℓ^*. Solidification of the interdendritic melt (Eq. (18)) increases c_d, while the expansion of the grain decreases c_d by enclosing the new volume with a lower concentration $\bar{c}_{env}$.

In the presence of convection, Eq. (40) or Eq. (42) is not valid, but the idea to treat the interfacial species exchanges, i.e., Eqs. (37) and (38), applies.

In order to estimate the diffusive flux from the grain envelope into the bulk melt, the following expression is used:

$$J_\ell = D_\ell \frac{\bar{c}_{env} - c_\ell}{l_\ell} \tag{43}$$

Several alternatives are suggested for evaluation of the diffusion length l_ℓ: (i) Zener-type diffusion, as mentioned in Ref. [5], $l_\ell = D_\ell / v_{R_e}$; (ii) the Landau transformation based on the numerical solution of the local diffusion field in the extradendritic melt [3,8]; (iii) the WB approach [9,30], which is based on the analytical solution of the diffusion field with an imposed condition that the integrated solute concentration of the extradendritic melt must be equal to c_ℓ; and (iv) the

approach suggested by Badillo and co-workers [26,27], where an experimentally determined Sherwood number correlation is used (the diffusion length is related to the grain size, Reynolds and Schmidt numbers of the settling grain). From a practical point of view, approach (iv) seems to be the most realistic, because the impact of melt flow on the solute diffusion boundary layer surrounding a grain is considered. Encouragingly, the succinonitrile (SCN)–acetone experiment has shown that the average growth velocity of the six primary dendrite tips is found to be in almost perfect agreement with the prediction from the standard free dendrite growth theory. However, the NH_4Cl–H_2O experiment has shown that the average growth velocity of the dendrite tips is ~15–68 times larger than that predicted by the free dendrite growth theory [24,25]. These contradicting results suggest that further experimental studies are necessary. The empirical Sherwood number correlation obtained for the organic model system SCN–acetone may not be valued for metallic alloys [26,27].

Approaches (ii) and (iii) are quite computationally expensive, and only valid without melt convection. Method (i) is not subjected to this restriction, but it may raise another concern. Normally for an alloy with $k < 1$, the extradendritic melt is gradually enriched with solute during solidification, given that the grain solidifies in an isolated "cell". If the species diffusive flux at the grain envelope is underestimated (e.g., $\rho_\ell \cdot S_e^D \cdot J_\ell < \rho_\ell \cdot (\bar{c}_{env} - c_\ell) \cdot df/dt$) because of an erroneous estimation of l_ℓ, the extradendritic melt concentration c_ℓ would decrease with solidification. This happens in particular for the case when the interdendritic melt is assumed to be well mixed ($c_d = c_\ell^* = \bar{c}_{\ env}$) and the diffusion area S_e^D is underestimated. To avoid this problem, an additional criterion ($l_\ell \leqslant D_\ell / v_{R_e}$) must be fulfilled [9].

An important issue, to which not enough attention was paid in previous works, is the consideration of the "true" diffusion surface area S_e^D. Most previous studies assumed a volume equivalent sphere to represent the volume within the "natural" contour of the grain. The volume equivalent sphere has a smaller surface area in comparison with any arbitrary shape of the "natural" grain contour. This assumption would facilitate the calculation of mass transfer (see Eq. (31)). However, if one takes the area of the volume equivalent sphere S_e^M for the calculation of the species diffusive flux, the diffusive flux will be underestimated. The real diffusion surface area of the "natural" grain contour is much larger than the surface area of the volume equivalent sphere S_e^M. The diffusion area is not equal to the artificial equivalent sphere and must be adjusted by a factor of Φ_{sph}, as expressed in Eq. (32). Based on this, together with the non-uniform interdendritic melt region, using the formula $l_\ell = D_\ell / v_{R_e}$, the species diffusive flux can be approximated in the current model.

Finally, the average concentration of the grain envelope $\bar{c}_{env}$ can be calculated according to the diffusion flux balance at the envelope:

$$D_d \cdot \frac{c_d - \bar{c}_{env}}{l_d} = D_\ell \cdot \frac{\bar{c}_{env} - c_\ell}{l_\ell} \tag{44}$$

which is similar to the expression of the WB model [9]:

$$\bar{c}_{env} = \frac{l_d c_\ell + l_\ell c_d}{l_d + l_\ell} \tag{45}$$

5. Solution procedure

A diversity of computational tools for solving a Eulerian multiphase transport system are available, each with their advantages and disadvantages [31–35]. The model discussed in the present paper is developed within the framework of the CFD software package, FLUENT (Fluent Inc. USA) [22]. FLUENT provides a platform for solving the global governing equations and provides flexibility in defining additional exchange and source terms for the governing equations, including modification of the transport quantities. For each time step, up to 60 iterations may be necessary to decrease the normalized residuals of continuity, momentum conservation, volume fraction, species transport and user-defined scalar conservation equations to a value below the convergence limit of 10^{-4}, and the enthalpy conservation equations below that of 10^{-7}. In each iteration, the intermediate (auxiliary) quantities, e.g., mixture concentration c_{mix}, the diameters of grains d_e are updated first. Based on the quantities of the last iteration, the exchange terms and the source terms are estimated. However, owing to the complexity of the multiphase coupling, the discretized linear equation system must be solved iteratively. The time step Δt should be kept small (~10^{-3}–10^{-4}) to ensure that the above convergent criteria are fulfilled. The optimal time step must be determined empirically by trial simulations or by using dynamic time step control.

6. Summary

A modified equiaxed solidification model with convection and grain sedimentation is proposed based on a previous globular equiaxed solidification model [13,14] with an extension to include the dendritic growth [1,9]. The improved modeling features are addressed as follows.

1. The grain starts to grow with globular morphology, and its growth is approximated by a Zener-type diffusion model for steady-state growth of a sphere. After the GDT, the growth of the dendritic grain is governed by the tip growth kinetic, e.g., LGK model. GDT is determined simply by comparison of the Zener-type diffusion growth velocity and the growth velocity of the volume equivalent sphere deduced from dendritic tip growth kinetics (maximum growth hypothesis).
2. Two morphological parameters were suggested to model the arbitrary dendritic grain morphology: the shape factor $\Phi_{\ env}$ and sphericity Φ_{sph}. The former, $\Phi_{\ env}$, is a factor relating the growth velocity of the volume equivalent sphere to the primary dendrite tip growth velocity, the later, Φ_{sph}, is the ratio of the surface area of the volume equivalent sphere to the surface area of the natural grain

contour. In reality, these morphological parameters are transient or process- and alloy-dependent quantities. Owing to the lack of detailed knowledge on these topics, they are assumed to be constant, i.e., the shape of the outer grain contour is preserved during dendritic growth.

3. Inside the dendritic grain, a non-uniform solute distribution in the interdendritic melt region is modeled. The average concentration of the interdendritic melt c_d is equal to neither the s–d interfacial concentration, which is the thermodynamic equilibrium concentration c_l^*, nor the grain envelope concentration $\bar{c}_{env}$. The difference between the interfacial concentration c_l^* and the average concentration c_d is considered as a driving force for the interdendritic melt solidification. The continuous solute distribution profile in the vicinity of the grain envelope is an important feature for quantitatively modeling the species exchange between the extra and interdendritic melts by the mechanisms of species diffusion and growth of the envelope.
4. The solidification of the interdendritic melt is governed by diffusion in the interdendritic melt region at the diffusion length scale of $\sim \lambda_2$. The uncertainty for the interdendritic diffusion length and its influence on the modeling accuracy will be studied and discussed in Part II.
5. Although three thermodynamic phases must be distinguished, only a two-phase Eulerian approach is applied to solve the transport system. The interdendritic melt and the solid dendrites, confined in the "natural" grain envelope, are regarded as one "hydrodynamic" phase, sharing the same velocity. It is only necessary to consider the hydrodynamic interaction between the extradendritic melt and the grains.

Illustrative modeling examples, theoretical and experimental verifications, and discussions on the uncertainty of the current model assumptions are presented in the companion paper: Part II.

References

[1] Rappaz M, Thévoz Ph. Acta Metall 1987;35:1478.
[2] Rappaz M, Thévoz Ph. Acta Metall 1987;35:2929.
[3] Appolaire B. Ph.D. Thesis, Institut National Polytechnique de Lorraine, France; 1999.
[4] Appolaire B, Combeau H, Lesoult G. Mater Sci Eng A 2008;487:33.
[5] Nielsen Ø, Appolaire B, Combeau H, Mo A. Metall Mater Trans 2001;32A:2049.
[6] Ciobanas AI, Fautrelle Y. J Phys D: Appl Phys 2007;40:3733.
[7] Ciobanas AI, Fautrelle Y. J Phys D: Appl Phys 2007;40:4310.
[8] Rappaz M, Boettinger WJ. Acta Mater 1999;47:3205.
[9] Wang CY, Beckermann C. Metall Trans 1993;24A:2787.
[10] Wang CY, Beckermann C. Metall Mater Trans 1996;27A: 2754.
[11] Wang CY, Beckermann C. Metall Mater Trans 1996;27A:2765.
[12] Beckermann C, Wang CY. Metall Mater Trans 1996;27A:2784.
[13] Ludwig A, Wu M. Metall Mater Trans 2002;33A:3673.
[14] Wu M, Ludwig A, Bührig-Polaczek A, Fehlbier M, Sahm PR. Int J Heat Mass Transfer 2003;46:2819.
[15] Wu M, Ludwig A. Metall Mater Trans 2006;37A:1613.
[16] Ludwig A, Wu M. Mater Sci Eng A 2005;109:413–4.
[17] Wu M, Ludwig A. Int J Cast Metals Res 2009;22:323.
[18] Gray DD, Giorgini A. Int J Heat Mass Transfer 1976;19(5):545.
[19] Rappaz M. Int Mater Rev 1989;34:93.
[20] Kurz W, Fisher DJ. Fundamentals of solidification. 4th ed. Zurich: TransTech; 1998.
[21] Lipton J, Glicksman ME, Kurz W. Mater Sci Eng 1984;65:57.
[22] Fluent 6.3 User's Guide. Lebanon, NH, USA: Fluent Inc.; September 2006.
[23] Ishii M, Zuber N. AIChE J 1979;25:843.
[24] Appolaire B, Albert V, Combeau H, Lesoult G. Acta Mater 1998;46:5851.
[25] Appolaire B, Albert V, Combeau H, Lesoult G. ISIJ Int 1999;39:263.
[26] Badillo A, Ceynar D, Beckermann C. J Crystal Growth 2007;309:197–215.
[27] Badillo A, Ceynar D, Beckermann C. J Crystal Growth 2007;309:216–24.
[28] Wang CY, Ahuja S, Beckerman C, de III HC. Metall Mater Trans 1995;26B:111.
[29] Mortensen A. Metall Trans 1991;22A:569.
[30] Martorano MA, Beckermann C, Gandin Ch-A. Metall Mater Trans 2003;34A:1657.
[31] Kolev N. Multiphase flow dynamics I: fundamentals. Berlin: Springer Verlag; 2002.
[32] Kolev N. Multiphase flow dynamics 2: mechanical and thermal interactions. Berlin: Springer Verlag; 2002.
[33] Patankar SV. Numerical heat transfer and fluid flow. Washington (DC): Hemisphere; 1980.
[34] Brennen CE. Fundamentals of multiphase flow. Cambridge: Cambridge University Press; 2005.
[35] Patankar SV. Numerical heat transfer and fluid flow. New York: Hemisphere; 1980.